Atmos. Meas. Tech. Discuss., 6, 911–948, 2013
www.atmos-meas-tech-discuss.net/6/911/2013/
doi:10.5194/amtd-6-911-2013

Atmospheric Measurement Techniques Discussions

Evaluation of the Lidar/Radiometer Inversion Code (LIRIC) to determine microphysical properties of volcanic and desert dust

J. Wagner[1], A. Ansmann[1], U. Wandinger[1], P. Seifert[1], A. Schwarz[1], M. Tesche[2], A. Chaikovsky[3], and O. Dubovik[4]

[1]Leibniz Institute for Tropospheric Research, Leipzig, Germany
[2]Department of Environmental Science, Stockholm University, Stockholm, Sweden
[3]Institute of Physics, National Academy of Science, Minsk, Belarus
[4]Laboratory of Atmospheric Optics, University Lille 1, Villeneuve d'Ascq, France

Received: 18 December 2012 – Accepted: 15 January 2013 – Published: 25 January 2013

Correspondence to: A. Ansmann (albert@tropos.de)

Published by Copernicus Publications on behalf of the European Geosciences Union.

Abstract

The Lidar/Radiometer Inversion Code (LIRIC) combines the multiwavelength lidar technique with sun-sky photometry and allows us to retrieve vertical profiles of particle optical and microphysical properties, separately for fine-mode and coarse-mode particles. After a brief presentation of the theoretical background, we evaluate the potential of LIRIC to retrieve the optical and microphysical properties of irregularly shaped dust particles. The method is applied to two very different aerosol scenarios, a strong Saharan dust outbreak towards central Europe and an Eyjafjallajökull volcanic dust event. LIRIC profiles of particle volume and mass concentrations are compared with results obtained with the polarization-lidar-based POLIPHON method. LIRIC profiles of optical properties such as particle backscatter coefficients, lidar ratio, Ångström exponent, and particle depolarization ratio are compared with direct Raman lidar observations. Good agreement between the different results are found for most of the retrieval products.

1 Introduction

The recent Icelandic volcanic eruptions in 2010 and 2011 emphasized the importance of remote-sensing methods that allow the separation of fine-mode and coarse-mode particles in the troposphere as a function of height (Ansmann et al., 2011, 2012). From the point of view of atmospheric research, there is a strong request for vertically resolved observations of optical and microphysical properties of atmospheric aerosols to improve our understanding of direct and indirect effects of aerosols on climate-relevant processes. The effects can be very different in the polluted boundary layer (dominated by local and regional aerosols) and in the free troposphere (controlled by long-range aerosol transport).

Presently efforts are undertaken to make complementary use of different measurement techniques such as lidar and sun-sky photometry at combined European Aerosol Research Lidar Network (EARLINET) and Aerosol Robotic Network (AERONET)

AMTD
6, 911–948, 2013

stations. The recently developed Lidar/Radiometer Inversion Code (LIRIC) analysis profiles of elastic-backscatter signals measured with multiwavelength lidar and spectrally-resolved column-integrated particle optical properties from photometer observations in a synergistic way (Chaikovsky et al., 2008, 2012). LIRIC was designed as a universal code for processing of lidar/photometer network data, applicable to many different instrumental conditions and technical approaches. The main purpose is the retrieval of height distributions of optical and microphysical properties of fine-mode and coarse-mode particles. LIRIC (as well as the AERONET data analysis code) searches for the minimum in the bimodal particle size distribution (volume number concentration) in the particle radius range from 0.194 µm–0.576 µm. The found minimum is used as a separation radius between fine- and coarse-mode particles. In this contribution, we present two case studies to discuss the potential of LIRIC to accurately determine the optical and microphysical aerosol properties of irregularly shaped dust particles. LIRIC assumes that dust particles are spheroidal particles. Müller et al. (2012) suggest that this assumption may introduce significant discrepancies in the retrieval products.

The inversion of sky radiance measurements within AERONET to obtain microphysical aerosol properties is well established (Dubovik and King, 2000; Dubovik et al., 2002a,b, 2006). The method also accounts for non-spherical particles by use of a spheroidal particle model and distinguishes fine-mode and coarse-mode particle fractions. Besides microphysical particle products, column values of the volume-specific backscatter and extinction coefficients of the particles can be estimated. These volume-specific backscatter and extinction values are important input data for LIRIC. The method is based on the Least Square Method (LSM) for statistically optimized inversion of multi-source data and has been developed in a cooperation between the Institute of Physics Minsk (Belarus) and the Laboratoire d'Optique Atmosphérique Lille (France) (Chaikovsky et al., 2008, 2012). LIRIC was originally designed for the analysis of lidar measurements at the three wavelengths of 355, 532, and 1064 nm. It has been extended to cover polarization lidar observations as well.

AMTD
6, 911–948, 2013

An alternative approach to separate fine-mode and coarse-mode particles as a function of height is the Polarization Lidar Photometer Networking (POLIPHON) method (Ansmann et al., 2011, 2012). The POLIPHON technique allows the separation of the contributions of spherical particles (mostly fine-mode particles) and non-spherical particles (mostly coarse-mode particles) to the measured optical effects. This method is based on directly measured linear particle depolarization ratios.

We focus on two cases with aerosol layers containing a considerable amount of irregularly shaped coarse-mode particles to test the potential of LIRIC in these cases with undefined particle shape characteristics and to compare the results with respective POLIPHON findings. The first case refers to a strong Saharan dust outbreak towards Europe in May 2008. The second case covers the aerosol conditions after the eruption of the Icelandic volcano Eyjafjallajökull in April 2010.

Section 2 describes the measurement systems. The LIRIC method is explained in Sect. 3. In addition, the basic idea of the POLIPHON method is briefly outlined. In Sect. 4, results are presented and discussed. Section 5 contains summarizing and concluding remarks.

2 Measurement systems

2.1 Raman lidar MARTHA

The multiwavelength Raman lidar MARTHA (Multiwavelength Atmospheric Raman lidar for Temperature, Humidity, and Aerosol profiling) is used for regular aerosol observations at the EARLINET station of Leipzig (Mattis et al., 2004). It provides height profiles of particle backscatter and extinction coefficients, lidar ratios as well as the volume and particle depolarization ratio at 532 nm (Ansmann et al., 1992, 2011). Because Raman lidar signals are used (in addition to elastic-backscatter signals), the method works best at darkness in the absence of strong sky background radiation. However, during events with optically dense aerosol layers, the Raman-lidar method for separate

AMTD
6, 911–948, 2013

extinction and backscattering profiling can even be applied during daylight hours, as will be shown in Sect. 4.

For LIRIC, the elastically backscattered signals at the three transmitted wavelengths of 355, 532, and 1064 nm and the cross-polarized signal at 532 nm are used. MARTHA transmits linearly polarized laser light at 532 nm and has two channels to measure the cross-polarized lidar return signal $P^{\perp}(\lambda, z)$ (the polarization-sensitive filter element is aligned orthogonal to the plane of laser beam polarization) and the total (cross and parallel-polarized) backscatter light $P^{\perp}(\lambda, z) + P^{\parallel}(\lambda, z)$ with a second channel. From these signals the depolarization ratio (introduced in the next section) can be determined.

For an optimum application of the LIRIC method, i.e. combining tropospheric column with tropospheric profile information, it is necessary that the lidar covers almost the entire tropospheric column (as seen by the photometer) with profile observations. However, the incomplete overlap between the transmitted laser beams and the receiver field-of-view (RFOV) prohibits the measurement of reliable lidar return signals in the near field (up to about 3 km above the lidar). The overlap function is routinely and regularly determined during clear nights with low aerosol amount by means of the method discussed by Wandinger and Ansmann (2002). These overlap functions are then applied to the aerosol lidar observations and allow us to correct the overlap effect usually down to heights of 500–1000 m above the lidar. At favorable conditions (as for the Saharan dust case presented here), the overlap correction is reliable down to low minimum measurement heights of 150 m.

2.2 Sun-sky photometer

Sun-sky photometers applied by AERONET detect direct sun, aureole, and sky radiance (Holben et al., 1998). At Leipzig, direct sun radiation is measured in eight channels from 340 to 1640 nm, whereas sky radiation is obtained in four bands from 440 to 1020 nm. From direct sun measurements the AOT and the Ångström exponent, which describes the wavelength dependence of the AOT, can be derived. Sky radiance

AMTD
6, 911–948, 2013

observations are used for inversion algorithms to retrieve microphysical aerosol properties such as the volume particle size distribution (Dubovik and King, 2000; Dubovik et al., 2006). Furthermore, the complex refractive index and the contribution of spherical particles can be determined. Based on these microphysical properties, AERONET provides the optical characteristics (the AOT, the column volume concentrations in $\mu m^3\,\mu m^{-2}$, phase functions, and asymmetry parameters) separately for the fine mode and the coarse mode (Dubovik et al., 2002a). In a case when sky radiance observations are not available the AOT and the column volume concentrations are derived from spectral dependence of measured total AOT of aerosol for both fine and coarse mode (O'Neill et al., 2003).

3 Method

3.1 Data preparation and processing

The basic structure of LIRIC is shown in Fig. 1. In order to run LIRIC the lidar data have to be prepared in the following way: The lidar database consists of background-corrected, elastic-backscatter lidar signals $P(\lambda_j, z_i)$ for different laser wavelengths λ_j:

$$P(\lambda_j, z_i) = E_0(\lambda_j)\frac{O(\lambda_j, z_i)}{z_i^2}[\beta_{\text{aer}}(\lambda_j, z_i) + \beta_{\text{mol}}(\lambda_j, z_i)] \times \exp\left[-2\int_0^{z_i}(\alpha_{\text{aer}}(\lambda_j, z) + \alpha_{\text{mol}}(\lambda_j, z))\mathrm{d}z\right]. \quad (1)$$

E_0 is the system constant and considers, e.g. the outgoing laser pulse energy, collection area of the telescope, optical efficiencies of the transmitter and receiver units, photon detection efficiency, and vertical thickness Δz of the backscattering range cell. $O(\lambda_j, z_i)$ describes the incomplete overlap of the laser beam for wavelength λ_j with the

AMTD
6, 911–948, 2013

RFOV. z_i denotes the vertical range between the lidar and the backscattering range cell. β_{aer} and β_{mol} are the particle and Rayleigh backscatter coefficients, respectively, and α_{aer} and α_{mol} the particle and Rayleigh extinction coefficients. The near-range measurements are influenced by the changing laser-beam RFOV overlap. This effect is corrected by use of measured overlap functions $O(\lambda_j, z_i)$ as mentioned in Sect. 2.1.

After range and overlap correction the signals are averaged over a given time period (of minutes to hours) to increases the signal-to-noise ratio. The corrected lidar signal

$$P_{\text{cor}}(\lambda_j, z_i) = \frac{P(\lambda_j, z_i) z_i^2}{O(\lambda_j, z_i)} \tag{2}$$

is used as basic lidar input in the LIRIC data analysis. The minimum measurement height z_{N_0} and the reference height z_N must be defined. Below z_{N_0}, the retrieval assumes constant microphysical and height-independent particle backscatter and extinction conditions as large as the values observed at the minimum measurement height (Mattis et al., 2004). Above z_N the contribution of aerosol particles to the AOT is assumed to be negligible. At the reference height z_N (usually at heights > 5 km) pure molecular backscattering conditions are typically given at the laser wavelengths of 355 and 532 nm. The following quantity is then introduced in the LIRIC procedure (see Fig. 1, green box):

$$L^*(\lambda_j, z_n) = \frac{P_{\text{cor}}(\lambda_j, z_n)}{P_{\text{cor}}(\lambda_j, z_N)} [\beta_{\text{aer}}(\lambda_j, z_N) + \beta_{\text{mol}}(\lambda_j, z_N)] \times \exp\left[-2 \sum_{i=N}^{n+1} \alpha_{\text{mol}}(\lambda_j, z_i) \Delta z\right] \tag{3}$$

$$= [\beta_{\text{aer}}(\lambda_j, z_n) + \beta_{\text{mol}}(\lambda_j, z_n)] \times \exp\left[2 \sum_{i=N}^{n+1} \alpha_{\text{aer}}(\lambda_j, z_i) \Delta z\right]$$

with the vertical range cell Δz which describes the range resolution of the lidar measurement. $L^*(\lambda_j, z_n)$ can be easily computed from the measured signal ratios by using height profiles of Rayleigh backscatter and extinction coefficients. The actual molecular optical properties are obtained from atmospheric temperature and pressure profiles

AMTD
6, 911–948, 2013

by using a standard atmosphere model, information from a nearby radiosonde, or numerical weather prediction products. In this study, we applied the US standard atmosphere model and adjusted it to actual surface temperature and pressure observations. Furthermore, negligible particle backscattering at 355 and 532 nm is assumed at the reference height z_N. In the case of 1064 nm, we must however provide an estimate of particle backscattering to total backscattering at the reference height.

The calculation of $L^*(\lambda_j, z_n)$ starts from the reference height $z_n = z_{N-1}$ and proceeds step by step down the minimum measurement height z_{N_0}. Because the LIRIC code is designed as LSM-based statistically optimized retrieval procedure it requires covariance matrices of the lidar signal measurement errors. Details to the signal noise estimations for the observations cases shown here are given by Wagner (2012). To assure optimized profiles, the optimization process is performed within the error margins.

Equation (3) shows that $L^*(\lambda_j, z_n)$ is mainly determined by height profiles of particle optical properties. These aerosol profiles are estimated by means of aerosol products retrieved from the photometer observations. For this task, the expression $L(\lambda_j, z_n)$ similar to $L^*(\lambda_j, z_n)$ from Eq. (3) is introduced (see Fig. 1, orange box):

$$L(\lambda_j, z_n) = [\beta_{\text{aer,e}}(\lambda_j, z_n) + \beta_{\text{mol}}(\lambda_j, z_n)] \times \exp\left[2 \sum_{i=N}^{n+1} \alpha_{\text{aer,e}}(\lambda_j, z_i) \Delta z\right]. \quad (4)$$

The particle backscatter and extinction coefficients $\beta_{\text{aer,e}}$ and $\alpha_{\text{aer,e}}$ (index e for estimate from photometer observations) are defined as

$$\beta_{\text{aer,e}}(\lambda, z) = C_{\text{f},1}(z) b_{\text{f},1}(\lambda) + C_{\text{f},2}(z) b_{\text{f},2}(\lambda) + C_{\text{c},1}(z) b_{\text{c},1}(\lambda) + C_{\text{c},2}(z) b_{\text{c},2}(\lambda), \quad (5)$$

$$\alpha_{\text{aer,e}}(\lambda, z) = C_{\text{f},1}(z) a_{\text{f},1}(\lambda) + C_{\text{f},2}(z) a_{\text{f},2}(\lambda) + C_{\text{c},1}(z) a_{\text{c},1}(\lambda) + C_{\text{c},2}(z) a_{\text{c},2}(\lambda) \quad (6)$$

with the particle volume concentrations $C_{m,s}(z)$ for particle mode m (index f for fine mode and index c for coarse mode) and particle shape parameter s with $s = 1$ for spherical particles and $s = 2$ for non-spherical particles. $C_{m,s}(z)$ are the variables that have to be optimized in the LIRIC data analysis. The procedure is outlined in detail

AMTD
6, 911–948, 2013

in Chaikovsky et al. (2008, 2012) and Wagner (2012). In Eqs. (5) and (6), the column mean values of the volume-specific particle backscattering b and extinction coefficient a are defined as (see Fig. 1, yellow boxes to the left)

$$b_{m,s}(\lambda) = \frac{4\pi\tau_{\text{ext},m,s}(\lambda)}{\omega_{m,s}(\lambda)F_{11,m,s}(\lambda,\Theta = 180°)V_{m,s}}, \quad (7)$$

$$a_{m,s}(\lambda) = \frac{\tau_{\text{ext},m,s}(\lambda)}{V_{m,s}}. \quad (8)$$

$b_{m,s}(\lambda)$ can be expressed by $a_{m,s}(\lambda)/S_{m,s}(\lambda)$ with the extinction-to-backscatter ratio (lidar ratio)

$$S_{m,s}(\lambda) = \frac{4\pi}{\omega_{m,s}(\lambda)F_{11,m,s}(\lambda,\Theta = 180°)}. \quad (9)$$

From photometric measurements (see Fig. 1, yellow box) the retrieved fine-mode and coarse-mode volume concentrations $V_{m,s}$, the complex refractive index (real part n_r, imaginary part n_i), the size distribution, and the fractions of spherical and non-sphercial particles are required to solve Eqs. (7) and (8). These quantities are obtained by means of the AERONET inversion algorithm. The non-spherical particles are assumed to have a spheroidal shape. A fixed fraction ratio of spherical to spheroidal particles is assumed for the fine mode in order to keep the set of input parameters as small as possible. Under the assumption of randomly oriented spheroids the first element of the scattering matrix F_{11}, the extinction optical thickness τ_{ext}, and the single-scattering albedo ω are provided for the lidar wavelengths by solving the vector radiative-transfer equation for a plane-parallel multi-layered atmosphere (Dubovik et al., 2006).

Besides the elastic backscatter signals for 355, 532, and 1064 nm, the cross-polarized 532-nm backscatter signal (denoted as 532c in Fig. 1, wavelength index $j = 4$) belongs to the LIRIC input signal data set. Only non-spherical particles cause light depolarization and thus contribute to the signal strength of the cross-polarized

AMTD
6, 911–948, 2013

channel. Consequently, the cross-polarized signal contains information on the fraction and amount of non-spherical particles.

As part of the optimization process the difference between the AERONET-related expression $L(\lambda_j, z_n)$ and the lidar-derived expression $L^*(\lambda_j, z_n)$ is minimized (Fig. 1, orange box, center). Also, the photometer-derived column volume concentrations $V_{m,s}$ must agree with the corresponding integrals over the respective concentration profiles (Fig. 1, orange box, center):

$$V_{m,s} = C_{m,s}(z_{N_0}) z_{N_0} + \sum_{i=N_0}^{N} [C_{m,s}(z_i)] \Delta z \,. \tag{10}$$

Here, $C_{m,s}(z_{N_0}) z_{N_0}$ describes the contribution of the lowermost tropospheric layer (below the lowermost lidar measurement height z_{N_0}) to the volume concentration profile. For heights $< z_{N_0}$ the values are set constant and equal to the value at z_{N_0}.

The retrieval is designed as statistically optimized fitting of multi-source data and uses multi-term LSM formulation (see detailed description in Dubovik, 2004). As a result, the retrieval is organized as minimization of a quadratic functional that consists of several terms, i.e. three expressions that describe the conformity of measured and recalculated lidar signals, the consistency between photometric measurements and retrieved concentration profiles, as well as smoothness constraints. This minimization procedure is not discussed in detail here. More information about the underlying numerical process can be found in Chaikovsky et al. (2008, 2012) and Wagner (2012).

In the derivation of the basic functional, regularization parameters are applied. These regularization parameters can be set and changed manually in order to find the best (optimum) solution. By slight adjustments of these parameters several sets of solutions are produced. Usually only small deviations between the different concentration profiles are found. Similarly small deviations are found when the minimum and reference heights or other input parameters are varied. The output data resulting from the variation of the regularization parameters is used for error estimation. The findings presented in the result section are based on 5–10 LIRIC runs. The mean value of the

AMTD
6, 911–948, 2013

different solutions is presented and the error bar indicates the standard deviation of the 5–10 different solutions.

Finally, the mass concentrations $M_f(z)$ and $M_c(z)$ for fine-mode and coarse-mode particles, respectively, can be calculated from the particle volume concentrations $C_{m,s}(z)$:

$$M_f(z) = \rho_1 C_{f,1}(z) + \rho_2 C_{f,2}(z), \quad (11)$$

$$M_c(z) = \rho_1 C_{c,1}(z) + \rho_2 C_{c,2}(z). \quad (12)$$

Estimates of the particle densities ρ_1 and ρ_2 (assumed to be height-independent) are required. Appropriate values of ρ_1 (mainly sulfate aerosol) and ρ_2 (desert and volcanic dust) can be found, e.g. in Ansmann et al. (2012). The final products of the LIRIC data analysis are summarized in the blue box in Fig. 1.

From the LIRIC backscatter and extinction coefficients after Eqs. (5) and (6), the lidar ratio profiles for the different wavelengths can be computed,

$$S_{aer,e}(\lambda, z) = \frac{\alpha_{aer,e}(\lambda, z)}{\beta_{aer,e}(\lambda, z)}. \quad (13)$$

Several Ångström exponents (Ångström, 1961),

$$\mathring{a}_{x_e}(\lambda_1, \lambda_2, z) = -\frac{\ln[x_e(\lambda_1, z)/x_e(\lambda_2, z)]}{\ln(\lambda_1/\lambda_2)} \quad (14)$$

with $\lambda_1 < \lambda_2$ can be calculated from the profiles of the particle backscatter ($x_e = \beta_{aer,e}$) and extinction coefficients ($x_e = \alpha_{aer,e}$).

The photometer data in combination with the applied particle scattering model (for spherical and spheroidal particles) permit the retrieval of column-mean backscatter coefficients as a function of the polarization state of the incident laser light:

$$b^{\perp}(\lambda) = b^{\perp}_{f,1}(\lambda) + b^{\perp}_{f,2}(\lambda) + b^{\perp}_{c,1}(\lambda) + b^{\perp}_{c,2}(\lambda), \quad (15)$$

$$b^{\parallel}(\lambda) = b^{\parallel}_{f,1}(\lambda) + b^{\parallel}_{f,2}(\lambda) + b^{\parallel}_{c,1}(\lambda) + b^{\parallel}_{c,2}(\lambda). \quad (16)$$

AMTD
6, 911–948, 2013

$\perp$ indicates here the plane of linear polarization perpendicular to the polarization plane of outgoing linearly polarized laser radiation pulses, whereas $\parallel$ stands for the polarization plane parallel to the laser light polarization plane. For spherical particles the contributions to light depolarization are negligible so that $b^{\perp}_{\mathrm{f},1}(\lambda) = 0$ and $b^{\perp}_{\mathrm{c},1}(\lambda) = 0$. As mentioned, only non-spherical particles (desert dust, volcanic dust) cause significant depolarization. Instead of Eq. (5), we can write

$$\beta^{\perp}_{\mathrm{aer,e}}(\lambda, z) = C_{\mathrm{f},2}(z) b^{\perp}_{\mathrm{f},2}(\lambda) + C_{\mathrm{c},2}(z) b^{\perp}_{\mathrm{c},2}(\lambda), \quad (17)$$

$$\beta^{\parallel}_{\mathrm{aer,e}}(\lambda, z) = C_{\mathrm{f},1}(z) b^{\parallel}_{\mathrm{f},1}(\lambda) + C_{\mathrm{f},2}(z) b^{\parallel}_{\mathrm{f},2}(\lambda) + C_{\mathrm{c},1}(z) b^{\parallel}_{\mathrm{c},1}(\lambda) + C_{\mathrm{c},2}(z) b^{\parallel}_{\mathrm{c},2}(\lambda) \quad (18)$$

so that we finally obtain the so-called particle linear depolarization ratio:

$$\delta_{\mathrm{aer,e}}(\lambda) = \beta^{\perp}_{\mathrm{aer,e}}(\lambda) / \beta^{\parallel}_{\mathrm{aer,e}}(\lambda). \quad (19)$$

The photometer-derived profiles of the lidar ratio, Ångström exponents, and depolarization ratio can be compared with the respective results directly determined from the Raman-lidar observations (Ansmann et al., 1992; Mattis et al., 2004; Tesche et al., 2009a). This comparison is presented in Sect. 4.

In conclusion, LIRIC uses photometer-derived volume-specific backscatter and extinction coefficients for spherical as well as non-spherical particles for both fine and coarse modes. This AERONET information (column-integrated values) is then applied to determine height profiles of volume and mass concentration of spherical and non-spherical fine-mode particles and spherical and non-spherical coarse-mode particles by minimizing the differences between the modelled lidar profiles $L(\lambda, z)$ and the measured lidar profiles $L^{*}(\lambda, z)$. The important point is that LIRIC is based on the assumption that non-spherical particles have a spheroidal shape. This may affect the backscatter-coefficient, lidar-ratio, and depolarization-ratio retrievals (Gasteiger et al., 2011; Müller et al., 2012), and thus potentially also the particle-volume and mass-concentration retrieval. The implication of the assumption of a spheroidal particle shape is discussed in the next section by comparing the LIRIC output with results obtained by means of the POLIPHON technique.

AMTD
6, 911–948, 2013

3.2 Determination of particle mass concentrations by means of the POLIPHON technique

An alternative approach for the retrieval of particle volume and mass concentration profiles is the single-wavelength POLIPHON technique (Ansmann et al., 2012). The method is based on measured profiles of the particle linear depolarization ratio and the lidar ratio at 532 nm and does not require the assumption of a specific particle shape. In this depolarization-ratio-based method it is assumed that the fine-mode-related backscatter and extinction coefficients are caused by non-light-depolarizing spherical particles (i.e. fine-mode fraction), and that the strongly light-depolarizing non-spherical particles are responsible for the optical properties related to the coarse mode. Spherical coarse particles as well as non-spherical fine-mode particles are ignored in this method. If the particle depolarization ratio is ≥ 0.31 in Saharan dust layers, the fine-mode particle fraction is set to 0 %. If the 532-nm depolarization ratio is ≤ 0.02, the coarse-mode fraction is set to 0 %. For depolarization ratios from 0.02 to 0.31 we use the method described by Tesche et al. (2009a) to compute the height profiles of the backscatter coefficient $\beta_{\mathrm{aer},1}$ of spherical particles and of $\beta_{\mathrm{aer},2}$ of non-spherical particles at $\lambda = 532$ nm. For volcanic dust, the data analysis is the same, except the volcanic depolarization ratio is set to 0.34 (Ansmann et al., 2012).

As it is the case for the LIRIC method, the POLIPHON technique makes use of photometer-derived volume-specific extinction coefficients a_{f} and a_{c} for fine- and coarse-mode particles (Eq. 8). The values for a_{f} and a_{c} can directly be computed from volume concentrations V_{f} and V_{c} and AOTs $\tau_{\mathrm{ext,f}}$ and $\tau_{\mathrm{ext,c}}$ downloaded from the AERONET website. The parameters a_{f} and a_{c} are almost insensitive to particle-shape effects, in contrast to scattering properties computed for a scattering angle of 180° (as required in the LIRIC data analysis in addition).

AMTD
6, 911–948, 2013

Finally, the mass concentrations M_1 for spherical particles (fine mode) and M_2 for non-spherical particles (coarse mode), respectively, are estimated:

$$M_1(z) = \rho_1 \overline{(V_f/\tau_{ext,f})} \beta_{aer,1}(z) S_{aer,1} \,,$$
$$= \rho_1 \overline{(a_f^{-1})} \beta_{aer,1}(z) S_{aer,1} \,, \quad (20)$$
$$M_2(z) = \rho_2 \overline{(V_c/\tau_{ext,c})} \beta_{aer,2}(z) S_{aer,2}$$
$$= \rho_2 \overline{(a_c^{-1})} \beta_{aer,2}(z) S_{aer,2} \,. \quad (21)$$

According to these equations, appropriate (actual) lidar ratios $S_{aer,1}$ and $S_{aer,2}$ are needed and obtained from the Raman lidar measurements or from combined photometer-lidar observations (Ansmann et al., 2011, 2012). Besides particle densities ρ_1 and ρ_2, temporal mean values of the volume-to-extinction conversion factors $\overline{V_{c,f}/\tau_{ext,c,f}}$ are determined and inserted in Eqs. (20) and (21).

The advantage of the POLIPHON method is that a particle shape model for irregularly shaped dust particles is not required. The particle depolarization ratio is used to separate spherical and non-spherical particle fractions. However, fine and coarse mode fractions as determined with LIRIC may not be well represented by these spherical and non-spherical particle fractions. A significant part of the non-spherical dust particles may belong to the fine mode, but are interpreted as coarse-mode particles when applying POLIPHON, i.e. when the non-spherical particle fraction is assumed to be identical with the coarse mode fraction. This aspect is further discussed in the next section.

4 Results

Two case studies are presented in the following. A strong Saharan dust outbreak reached central Europe in the end of May 2008. Fine-mode particles and coarse-mode

AMTD
6, 911–948, 2013

particles were almost perfectly separated with height. Urban haze occurred in the lowermost 700 m of the atmosphere, whereas desert dust was observed from 1–6 km height. Mixing was prohibited by a strong temperature inversion layer at the top of the haze layer. In contrast, the second case deals with an aged volcanically disturbed air mass without apparent layering observed over Leipzig after the Eyjafjallajökull volcanic eruption in April 2010. A mixture of sulfate particles of volcanic origin and volcanic dust dominated particle backscattering and extinction. These two observational cases were already discussed in detail by Ansmann et al. (2012) so that the LIRIC method can be applied to well-documented and quality-checked lidar/photometer data sets.

4.1 Saharan dust

A long-lasting Saharan dust event was monitored with lidar and photometer from 25–31 May 2008. The particle optical thickness at 500 nm showed values around 0.7 from the early morning of 28 May 2008 to the early morning of 30 May 2008. Figure 2 shows lidar height-time displays of the 1064-nm range-corrected signal in the evening of 29 May 2008. Well stratified dust layers up to 5.5 km were found. Persistent, long-lasting cirrus decks frequently occurred and disturbed the AERONET sun-sky photometer observations. A good opportunity to compare and combine lidar and photometer observations and to apply the LIRIC method was given in the evening of 29 May 2008. At around 17:30 UTC, the sky was cloud-free during several successive AERONET observations. Stable aerosol conditions throughout the following night enabled the determination of the full set of Raman lidar results and ensured a perfect framework for a critical assessment of the LIRIC results.

Lidar measurements in the evening of 29 May 2008, 21:47 to 23:15 UTC, were analyzed. The retrieved 1.5-h mean profiles of the three particle backscatter coefficients at 355, 532, and 1064 nm computed with Eq. (5) and the corresponding extinction profiles after Eq. (6) are presented in Fig. 3. In addition, the particle backscatter coefficient computed from the cross-polarized 532-nm backscatter signal is presented. This latter backscatter coefficient considers only backscattering by non-spherical particles

AMTD
6, 911–948, 2013

according to Eq. (17). Figure 3 also shows the corresponding profiles of the volume concentrations for fine-mode and coarse-mode particles as retrieved with LIRIC. As mentioned, the constraints here are that the vertically integrated fine- and coarse-mode volume concentrations must match the respective column values retrieved from the AERONET observations.

As outlined above, the lidar was well aligned on this day and the overlap function well characterized. The incomplete overlap between laser beam and RFOV could be corrected with sufficient accuracy down to z_{N_0} = 150 m height. The reference height z_N was set to 9 km height. The 500-nm AOT measured with the AERONET photometer was 0.73 at 17:30 UTC and 0.70 in the next morning.

The particle backscatter coefficients show a weak reversed spectral order (negative Ångström exponent) in the dust layer between 500 m and 5.5 km height and almost no wavelength dependence in terms of the extinction coefficient. In the pollution layer below 600 m height, a strong decrease of the backscatter and extinction coefficients with wavelength is found according to Ångström values of around 1.5. The volume concentration profiles show a dominant coarse particle mode in the height range from 600 m to 6 km. A volume concentration of 0.1 ppb corresponds to 100 $\mu m^3\,cm^{-3}$. The fine-mode particles predominantly occur in the boundary layer below 600 m and another weak accumulation of fine particles is found around 2 km. The LIRIC/AERONET analysis indicated the absence of spherical coarse-mode particles throughout the troposphere.

Figure 4 shows a comparison of the LIRIC backscatter coefficients at 532 nm with respective backscatter profiles directly retrieved from the Raman lidar observations (total backscatter coefficient, for simplicity denoted as POLIPHON curves) and derived by using the separation method of Tesche et al. (2009a) for the spherical and non-spherical particle fractions. As can be seen, the total backscatter coefficients agree well.

A systematic bias (lower LIRIC coarse-mode backscatter coefficients) is observed in the dust layer. Several reasons may have contributed to the deviation between the LIRIC and POLIPHON curves. According to Müller et al. (2012), spheroidal particles

AMTD
6, 911–948, 2013

produce a less pronounced 180° scattering peak than the irregularly shaped desert dust particles and may lead to an underestimation of the dust backscatter coefficient by up to 20 %. Another point is that backscatter coefficients of the coarse mode and of the non-spherical particles fraction are compared. The non-spherical particle fraction covers coarse-mode as well as fine-mode particles. Furthermore, the threshold depolarization ratio for pure dust of 0.31 (for this depolarization ratio, 100 % of the particles are assumed to be dust particles) in the POLIPHON analysis may be too low so that the fraction of non-spherical particles is overestimated. Finally, the volume-specific backscatter coefficient as derived from the AERONET observations (column value) and used as a proxy in the LIRIC analysis may not describe properly the height profile of the volume-specific backscatter coefficient that belongs to the measured lidar signal profiles. Variations in the dust size distribution and chemical composition cause respective variations in the volume-specific backscatter coefficients (around the column value given by AERONET). These variations then may introduce height variations in the LIRIC dust backscatter coefficients. Similarly, the threshold dust depolarization ratio of 0.31 may not be appropriate for all height levels in the Saharan dust plume and can introduce respective height variations in the POLIPHON dust backscatter coefficients.

The fine-mode backscatter coefficient computed from the fine-mode term in Eq. (5), on the other hand, is larger than the one obtained with POLIPHON at heights >1 km. This is consistent with the assumption that part of the non-spherical particles belong to the fine mode. Therefore, the POLIPHON backscatter coefficient for spherical particles does not represent the entire fine-mode backscatter coefficient. Another reason for the deviations may be that the assumed ratio of non-spherical to spherical particle for the fine-mode fraction is constant in the LIRIC analysis. It cannot be excluded that this ratio was to high, i.e. that the fraction of non-spherical fine-mode particles was much lower than assumed.

The results of the retrieval of the particle mass concentration by means of Eqs. (11) and (12) are shown in Fig. 5 (green curves) together with the profiles derived by using the POLIPHON method (Eqs. 20 and 21, blue curves). A dust particle density of

AMTD
6, 911–948, 2013

$\rho_2 = 2.6\,\mathrm{g\,cm^{-3}}$ and a fine-mode particle density of $\rho_1 = 1.6\,\mathrm{g\,cm^{-3}}$ are assumed in the calculation of the mass concentrations from the derived volume concentrations.

A very good agreement of the LIRIC and POLIPHON results is found. As mentioned in Sect. 3, the integral of the profile of the LIRIC coarse-mode volume concentration must match the AERONET-derived column value of the coarse-mode volume concentration. According to Fig. 5 obviously not only LIRIC but also the POLIPHON results are in good agreement with the AERONET column observations. One can conclude that the non-spherical particle fraction well represents the coarse mode in the particle volume and mass retrievals in this case of a strong Saharan dust outbreak.

The fine-mode volume and mass concentrations (LIRIC) are larger than the values for spherical particles retrieved by the POLIPHON approach. The disagreement is probably related to the fact that the non-spherical particles which belong to the fine mode are not considered in the POLIPHON curve.

Comparisons of the LIRIC and Raman lidar results in terms of lidar ratio, extinction-related Ångström exponent, and particle depolarization ratio are shown in Fig. 6. The 532-nm lidar ratios (LIRIC, Eq. 13) are determined by dividing the 532-nm extinction coefficients by the 532-nm backscatter values in Fig. 3. The Ångström exponents are computed from the 355-nm and 532-nm particle extinction coefficients after Eq. (14). In the case of the LIRIC particle depolarization ratios the backscatter coefficients computed from the cross-polarized and parallel-polarized signals shown in Fig. 3 are simply divided according to Eq. (19).

As can be seen, the particle lidar ratio in the dust layer is systematically overestimated by the LIRIC approach. This is in agreement with the discussion of the LIRIC and Raman-lidar backscatter coefficients. The use of the spheroidal particle model may lead to a less pronounced 180° scattering peak (by up to 20 %) than the one observed for irregularly shaped desert dust particles (Müller et al., 2012). On the other hand, the extinction computation is not affected (Dubovik et al., 2006). As a consequence, the extinction-to-backscatter ratio may be overestimated by up to 20 %. The directly observed lidar ratios are around 50–55 sr in Fig. 6. These values are typical for Saharan

AMTD
6, 911–948, 2013

dust (Tesche et al., 2009b). In the case of 355 and 1064 nm, the LIRIC backscatter and extinction profiles lead to lidar ratios of 78–80 sr and 54–55 sr, respectively, in the height range from 1500–3000 m (center part of the dust layer). This spectral dependence, not seen in the observations, also points to uncertainties in the LIRIC results by the applied spheroidal particle shape model.

The Ångström exponent retrieved with LIRIC fluctuates around zero in the dust layer and fits well to the respective results obtained from the direct Raman lidar observations. The very low values clearly indicate the dominance of coarse-mode particles in the lofted Saharan dust plume.

Particle depolarization ratio profiles are also in good agreement, despite the fact that the spheroidal model may also lead here to an underestimation of the 532-nm particle depolarization ratio by up to 20 % (Müller et al., 2012). The LIRIC approach tries to obtain best agreement between the input profiles (cross- and total, i.e. cross- + parallel-polarized lidar signals) and the retrieved backscatter coefficients (for cross-polarized and total backscatter channels). This optimization process obviously leads to well reproduced lidar signals, backscatter coefficients, and respective depolarization ratio.

4.2 Volcanic ash on 19 April 2010

In April 2010, an aged volcanic aerosol layer consisting of a mixture of volcanic dust, volcanic sulfate particles, and anthropogenic haze occurred over central Europe. These aerosol conditions provided an unique opportunity to apply the LIRIC approach to another type of irregularly shaped aerosol particles. In contrast to desert dust, volcanic dust is hygroscopic (Lathem et al., 2011) so that changes in the shape characteristics by water uptake cannot be excluded when relative humidity is high (e.g. > 70 %) (Ansmann et al., 2012). As a consequence, spherical particles may occur not only in the fine-mode, but also in the coarse-mode fraction, and thus may complicate the interpretation of POLIPHON results and the comparison with LIRIC results.

AMTD
6, 911–948, 2013

The volcanic layers observed on 19 April 2010 originated from the Eyjafjallajökull volcanic eruptions on Iceland on 14 April 2010 (Ansmann et al., 2011; Schumann et al., 2011). Figure 7 shows the situation in the afternoon of 19 April 2010. The 500-nm AOT was about 0.7 and thus a factor of 2–3 higher than usually observed for air mass transport from the west. The fine-mode 500-nm AOT of 0.5 was at least to 50 % caused by sulfate particles of volcanic origin (Ansmann et al., 2011). The well-mixed boundary layer reached to 1000–1400 m height on that day. Above the boundary layer occurred another layer of 1500 m thickness mainly consisting of volcanic dust. Between 3.8 and 5.5 km height a further dust layer was detected consisting of fine- and coarse-mode particles. At heights around 9 km a cirrus layer developed after 15:00 UTC. Photometer measurements at cloud-free conditions became almost impossible after 16:00 UTC.

Figure 8 shows the LIRIC products in terms of profiles of particle backscatter coefficient, extinction coefficient, and particle volume concentration for the fine-mode and the coarse-mode fraction. LIRIC calculations were performed with cloud-screened lidar signal profiles for the time period from 14:35–15:36 UTC on 19 April 2010. The considered photometric measurements were taken at 14:49 UTC. Lidar signals were only used up to 8.25 km height (reference point) because of cirrus cloud evolution above this height. The minimum measurement height z_{N_0} was set to 600 m.

According to the volume concentration profiles in Fig. 8, fine-mode particles prevailed in the lowermost 1 km of the troposphere (in the boundary layer). From 1–2 km height (at relative humidities around 60 %), a mixture of non-spherical coarse-mode volcanic dust particles and fine-mode spherical sulfate particles occurred. Above 2 km height, irregularly shaped coarse-mode volcanic dust particles dominated. A mixture of fine- and coarse-mode particles was detected in the lofted layer above 3.5 km height. Cumulus cloud development at around 13:45 UTC at 1 km height (see Fig. 7) indicates high relative humidity of >80 % close to the top of the boundary layer and thus particle water-uptake effects must be taken into account in the data interpretation. However, the LIRIC/AERONET analysis again did not indicate the occurrence of spherical particles

AMTD
6, 911–948, 2013

in the coarse mode. The relative humidity was about 60 % in the lofted layer from 1.5–2.8 km and less than 30 % in the layer above 3.5 km height (Ansmann et al., 2012).

The backscatter and extinction coefficients retrieved with LIRIC show a pronounced wavelength-dependence below 2 km and thus indicate a dominating fine-mode impact on the particle optical properties. Above 2 km the backscatter coefficients are nearly the same for all wavelengths. This is caused by the dominating coarse-mode particle fraction.

The comparisons of the LIRIC results with respective POLIPHON findings and Raman lidar observations of optical properties are shown in Figs. 9 to 11. These comparisons for the volcanic case are much more difficult to interpret than it was the case for the earlier described and simpler Saharan event. As mentioned, complex layering was found. Coarse-mode volcanic dust particles were mixed with fine-mode sulfate particles. The degree of mixing changed with height and strong gradients in the aerosol concentrations were observed. It is very likely that the height-independent volume-specific backscatter and extinction coefficients as derived from the AERONET observations for the different aerosol types (and thus particle sizes, shapes, and compositions) do not hold for all height levels adequately. Strong variations with height in the volume-specific optical properties and volume-to-extinction conversion ratios may have occurred. This would influence both the LIRIC as well as the POLIPHON results.

As can be seen in Fig. 9, the comparison of the profiles of the particle backscatter coefficients with the ones directly determined from the Raman lidar observations do not agree well. Part of the systematic deviations in the lowermost 2 km may be caused by an erroneous correction of the overlap effect. The LIRIC backscatter coefficients are based on the elastic backscatter signals and are thus very sensitive to uncertainties in the overlap correction. The Raman lidar backscatter values in Fig. 9 are calculated from signal ratios (ratio of elastic backscatter signal to nitrogen Raman signal) so that the overlap effect (affecting both signals in almost the same manner) widely cancels out.

AMTD
6, 911–948, 2013

The LIRIC coarse-mode backscatter coefficients in the layers from 2–3 km and 4–5.5 km height are lower than the POLIPHON backscatter values for non-spherical particles. This may be partly attributed to the application of the spheroidal particle model. The reason of the strong deviation of LIRIC fine-mode backscatter coefficients and POLIPHON spherical particle backscatter values at lower heights is unclear. Although the LIRIC/AERONET retrieval did not indicate spherical coarse mode particles, it cannot be excluded that some spherical volcanic dust particles formed at high humidity and significantly contributed to the spherical particle backscatter coefficient.

As can be seen in Fig. 10, the profiles of the volcanic dust mass concentrations, i.e. for the dry, irregularly shaped particles above 1.5 km height agree mostly within the error margins. Because the LIRIC profile is in full agreement with the AERONET column value, the POLIPHON mass concentrations are too high by about 20 %–50 % at heights above 2 km. The respective column value (POLIPHON) is 20 % higher than the AERONET column value. Most likely, the extinction-to-volume conversion factor (i.e. the volume-specific extinction coefficient) applied to the backscatter and extinction coefficients of the non-spherical particle fraction was too high. The uncertainty in this conversion factor is considered in the shown error bars.

Regarding the fine-mode mass concentrations, again the POLIPHON column value (integral over the profile) is 20 % higher than the respective AERONET column value. In the case of the LIRIC profile, the fine-mode mass concentration at heights <2 km appear to be systematically underestimated caused by an improper overlap correction (which increases with decreasing height). It can also not be excluded that a few coarse-mode particles with spherical shape were present at low heights (at high humidities) and increased the mass values derived with the POLPIPHON method. However, taking the error bars in Fig. 10 into consideration, the agreement is acceptable.

Figure 11 shows the comparison of the LIRIC results with the direct Raman lidar observations of the 532-nm lidar ratio, Ångström exponents computed from the Raman-lidar-derived particle extinction coefficients at 355 and 532 nm, and the particle depolarization ratio at 532 nm. Considering the complicated aerosol situation, the agreement

AMTD
6, 911–948, 2013

of the different profiles is surprisingly good. The underestimation of the lidar ratio for irregularly shaped particles (see values at 2.5 and 4.5 km height), as observed in the case of Saharan dust is not found. We conclude that the complex and manifold influences as discussed above have partly compensated each other and the different effects have been smoothed out.

5 Conclusions

The LIRIC method based on multiwavelength lidar and sun-sky photometer observations was applied to two very different aerosol scenarios to evaluate the potential for the retrieval of optical and microphysical properties of irregularly shaped dust particles. LIRIC aerosol profiles were compared with respective results obtained with the single-wavelength polarization lidar method POLIPHON and direct Raman lidar observation of basic particle optical properties.

The results for a well-stratified Saharan dust case in May 2008 and complex layering of volcanic aerosol in April 2010 indicated a good, trustworthy retrieval of the volume and mass concentration profiles of irregularly shaped coarse-mode particles with LIRIC. The assumed spheroidal shape of the dust particles may have partly lead to an underestimation of the particle backscatter coefficient and the extinction-to-backscatter ratio.

The presented two case studies demonstrate that LIRIC is a powerful tool for the retrieval of optical and microphysical aerosol properties. As raw and ready-to-use elastic backscatter lidar signals serve as input for the algorithm and photometric measurements are available through the AERONET website, an almost instantaneous and fast data analysis is possible. An automated version of LIRIC is currently under development. However, further sensitivity studies should be conducted. These should include cases with deep continental boundary layers, complex situations with biomass-burning smoke (from domestic fires, wild fires, or forest fires), and observations in areas that are strongly affected by marine particles such as coastal regions with sea-breeze effects.

AMTD
6, 911–948, 2013

The shortcoming of the majority of aerosol lidars to be unable to cover the lowermost, usually most polluted part of the atmosphere with aerosol observations needs to be further investigated. In general, the use of lidars with at least two receiver units for near-range and far-range observations is desirable to guarantee high-quality LIRIC products. Vice versa, small lidars such as ceilometers may cover the lowest heights only, but may be not able to provide proper aerosol observations in lofted layers in the middle and upper troposphere. LIRIC applications are difficult in these cases, too.

Acknowledgements. The research leading to these results has received funding from the European Union Seventh Framework Programme (FP7/2007-2013) under grant agreement no 262254.

References

Ansmann, A., Wandinger, U., Riebesell, M., Weitkamp, C., and Michaelis, W.: Independent measurement of extinction and backscatter profiles in cirrus clouds by using a combined Raman elastic–backscatter lidar, Appl. Opt., 31, 7113–7131, 1992. 914, 922

Ansmann, A., Tesche, M., Seifert, P., Groß, S., Freudenthaler, V., Apituley, A., Wilson, K. M., Serikov, I., Linné, H., Heinold, B., Hiebsch, A., Schnell, F., Schmidt, J., Mattis, I., Wandinger, U., and Wiegner, M.: Ash and fine-mode particle mass profiles from EARLINET-AERONET observations over central Europe after the eruptions of the Eyjafjallajökull volcano in 2010, J. Geophys. Res., 116, D00U02, doi:10.1029/2010JD015567, 2011. 912, 914, 924, 930, 941

Ansmann, A., Seifert, P., Tesche, M., and Wandinger, U.: Profiling of fine and coarse particle mass: case studies of Saharan dust and Eyjafjallajökull/Grimsvötn volcanic plumes, Atmos. Chem. Phys., 12, 9399–9415, doi:10.5194/acp-12-9399-2012, 2012. 912, 914, 921, 923, 924, 925, 929, 931, 941, 942, 946, 947

Chaikovsky, A., Dubovik, O., Goloub, P., Balashevich, N., Lopatsin, A., Karol, Y., Denisov, S., and Lapyonok, T.: Software package for the retrieval of aerosol microphysical properties in the vertical column using combined lidar/photometer data (test version), Tech. rep., Institute of Physics, National Academy of Sciences of Belarus, Minsk, Belarus, 2008. 913, 919, 920

AMTD
6, 911–948, 2013

Chaikovsky, A., Dubovik, O., Goloub, P., Tanré, D., Pappalardo, G., Wandinger, U., Chaikovskaya, L., Denisov, S., Grudo, Y., Lopatsin, A., Karol, Y., Lapyonok, T., Korol, M., Osipenko, F., Savitski, D., Slesar, A., Apituley, A., Arboledas, L. A., Binietoglou, I., Kokkalis, P., Granados Muñoz, M. J., Papayannis, A., Perrone, M. R., Pietruczuk, A., Pisani, G., Rocadenbosch, F., Sicard, M., De Tomasi, F., Wagner, J., and Wang, X.: Algorithm and software for the retrieval of vertical aerosol properties using combined lidar/radiometer data: Dissemination in EARLINET, in: Proceedings of the 26th International Laser and Radar Conference/26th International Laser and Radar Conference, vol. 1, Porto Heli, Greece, 25–29 June 2012, 399–402, 2012. 913, 919, 920

Dubovik, O.: Optimization of numerical inversion in photopolarimetric remote sensing, in: Photopolarimetry in Remote Sensing, edited by: Videen, G., Yatskiv, Y., and Mishchenko, M., Kluwer Academic Publishers, Dordrecht, The Netherlands, 65–106, 2004. 920

Dubovik, O. and King, M. D.: A flexible inversion algortihm for retrieval of aerosol optical properties from Sun and sky radiance measurements, J. Geophys. Res., 105, 20673–20696, 2000. 913, 916

Dubovik, O., Holben, B. N., Eck, T. F., Smirnov, A., Kaufman, Y. J., King, M. D., Tanré, D., and Slutsker, I.: Variability of absorption and optical properties of key aerosol types observed in worldwide locations, J. Atmos. Sci., 59, 590–608, 2002a. 913

Dubovik, O., Holben, B. N., Lapyonok, T., Sinyuk, A., Mishchenko, M. I., Yang, P., and Slutsker, I.: Non-spherical aerosol retrieval method employing light scattering by spheroids, Geophys. Res. Lett., 29, 1415, doi:10.1029/2001GL014506, 2002b. 913

Dubovik, O., Sinyuk, A., Lapyonok, T., Holben, B. N., Mishchenko, M., Yang, P., Eck, T. F., Volten, H., Munoz, O., Weihelmann, B., van der Zande, W. J., Leon, J.-F., Sokorin, M., and Slutsker, I.: Application of spheroid models to account for aerosol particle nonspericity in remote sensing of desert dust, J. Geophys. Res., 11, D11208, doi:10.1029/2005JD006619, 2006. 913, 916, 919, 928

Gasteiger, J., Wiegner, M., Groß, S., Freudenthaler, V., Toledano, C., Tesche, M., and Kandler, K.: Modelling lidar-relevant optical properties of complex mineral dust aerosols, Tellus B, 63, 725–741, 2011. 922

Holben, B. N., Eck, T. F., Slutsker, I., Tanré, D., Buis, J. P., Setzer, A., Vermote, E., Reagan, J. A., Kaufman, Y. J., Nakajima, T., Lavenu, F. Jankowiak, I., and Smirnov, A.: AERONET – A federated instrument network and data archive for aerosol characterization, Remote Sens. Environ., 66, 1–16, 1998. 915

AMTD
6, 911–948, 2013

Lathem, T. L., Kumar, P., Nenes, A., Dufek, J., Sokolik, I. N., Trail, M., and Russell, A.: Hygroscopic properties of volcanic ash, Geophys. Res. Lett., 38, L11802, doi:10.1029/2011GL047298, 2011. 929

Mattis, I., Ansmann, A., Müller, D., Wandinger, U., and Althausen, D.: Multiyear aerosol observations with dual-wavelength Raman lidar in the framework of EARLINET, J. Geophys. Res., 109, D13203, doi:10.1029/2004JD004600, 2004. 914, 917, 922

Müller, D., Lee, K.-H., Gasteiger, J., Tesche, M., Weinzierl, B., Kandler, K., Müller, T., Toledano, C., Otto, S., Althausen, D., and Ansmann, A.: Comparison of optical and microphysical properties of pure Saharan mineral dust observed with AERONET Sun photometer, Raman lidar, and in situ instruments during SAMUM 2006, J. Geophys. Res., 117, D07211, doi:10.1029/2011JD016825, 2012. 913, 922, 926, 928, 929

O'Neill, N. T., Eck, T. F., Smirnov, A., Holben, B. N., and Thulasiraman, S.: Spectral discrimination of coarse and fine mode optical depth, J. Geophys. Res., 108, 4559, doi:10.1029/2002JD002975, 2003. 916

Schumann, U., Weinzierl, B., Reitebuch, O., Schlager, H., Minikin, A., Forster, C., Baumann, R., Sailer, T., Graf, K., Mannstein, H., Voigt, C., Rahm, S., Simmet, R., Scheibe, M., Lichtenstern, M., Stock, P., Rüba, H., Schäuble, D., Tafferner, A., Rautenhaus, M., Gerz, T., Ziereis, H., Krautstrunk, M., Mallaun, C., Gayet, J.-F., Lieke, K., Kandler, K., Ebert, M., Weinbruch, S., Stohl, A., Gasteiger, J., Groß, S., Freudenthaler, V., Wiegner, M., Ansmann, A., Tesche, M., Olafsson, H., and Sturm, K.: Airborne observations of the Eyjafjalla volcano ash cloud over Europe during air space closure in April and May 2010, Atmos. Chem. Phys., 11, 2245–2279, doi:10.5194/acp-11-2245-2011, 2011. 930

Tesche, M., Ansmann, A., Müller, D., Althausen, D., Engelmann, R., Freudenthaler, V., and Groß, S.: Separation of dust and smoke profiles over Cape Verde by using multiwavelength Raman and polarization lidars during SAMUM 2008, J. Geophys. Res., 114, D13202, doi:10.1029/2009JD011862, 2009a. 922, 923, 926

Tesche, M., Ansmann, A., Müller, D., Althausen, D., Mattis, I., Heese, B., Freudenthaler, V., Wiegner, M., Esselborn, M., Pisani, G., and Knippertz, P.: Vertical profiling of Saharan dust with Raman lidars and airborne HSRL in southern Morocco during SAMUM, Tellus B, 61, 144–164, 2009b. 929

Wagner, J.: Microphysical properties retrieved from combined lidar sun photometer measurements, University Master Thesis, Universität Leipzig, Germany, Sächsische Landesbibliothek

AMTD
6, 911–948, 2013

– Staats- und Universitätsbibliothek Dresden, available at: http://nbn-resolving.de/urn:nbn:de:bsz:15-qucosa-99830, 2012. 918, 919, 920
Wandinger, U. and Ansmann, A.: Experimental determination of the lidar overlap profile with Raman lidar, Appl. Opt., 41, 511–514, 2002. 915

AMTD
6, 911–948, 2013

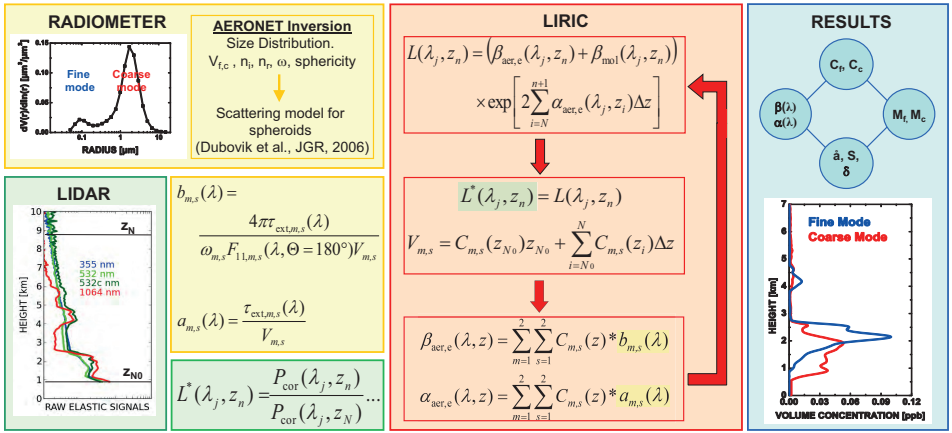

Fig. 1. Basic structure of LIRIC. Photometric information (radiometer, top yellow box) is used to retrieve height-independent (column) volume-specific backscatter and extinction coefficients $b_{m,s}$ and $a_{m,s}$ (center yellow box) for spherical (s = 1) and non-spherical particles (s = 2) of the fine mode ($m = f$) and coarse mode ($m = c$). A lidar signal term L (orange box, top) can be calculated with LIRIC by using profiles of backscatter and extinction coefficients (orange box, bottom) which, in turn, are calculated from the volume-specific coefficients $b_{m,s}$ and $a_{m,s}$ and profiles of particle volume concentration $C_{m,s}(z)$. Deviations between the observed lidar signal term L^* (green box) and the LIRIC expression L are minimized in order to retrieve optimized $C_{m,s}(z)$ profiles (orange box, center). As a constraint, the integrals of the $C_{m,s}(z)$ profiles must match the respective column values $V_{m,s}$ as observed with AERONET photometer (orange box, center). LIRIC products (blue box) are profiles of particle optical properties (e.g. backscatter and extinction profiles, Ångström exponents, lidar and depolarization ratios) and microphysical properties (e.g. volume concentrations C_f and C_c and respective mass concentrations M_f and M_c for fine and coarse mode).

AMTD
6, 911–948, 2013

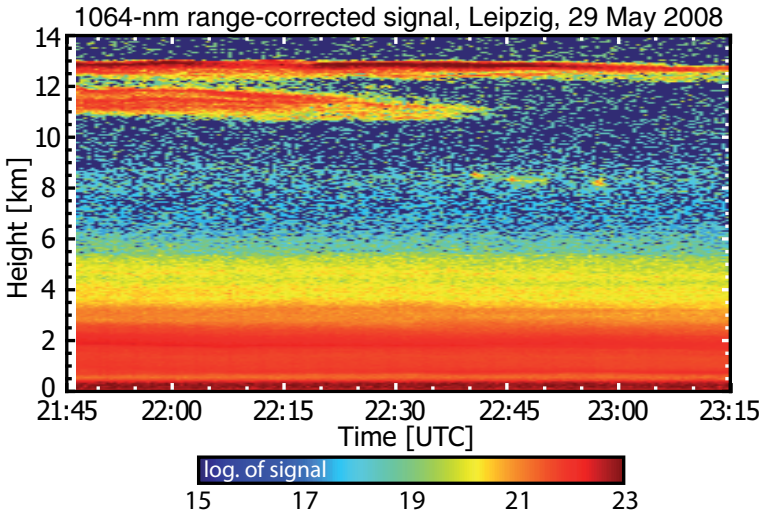

Fig. 2. Range-corrected signal at 1064 nm measured on 29 May 2008, 21:47–23:15 UTC (signal counts in logarithmic scale). The vertical resolution of the lidar measurement is 60 m, the temporal resolution is 30 s. The 500-nm AOT was 0.70–0.75 up to 6 km height in the evening of 29 May.

AMTD
6, 911–948, 2013

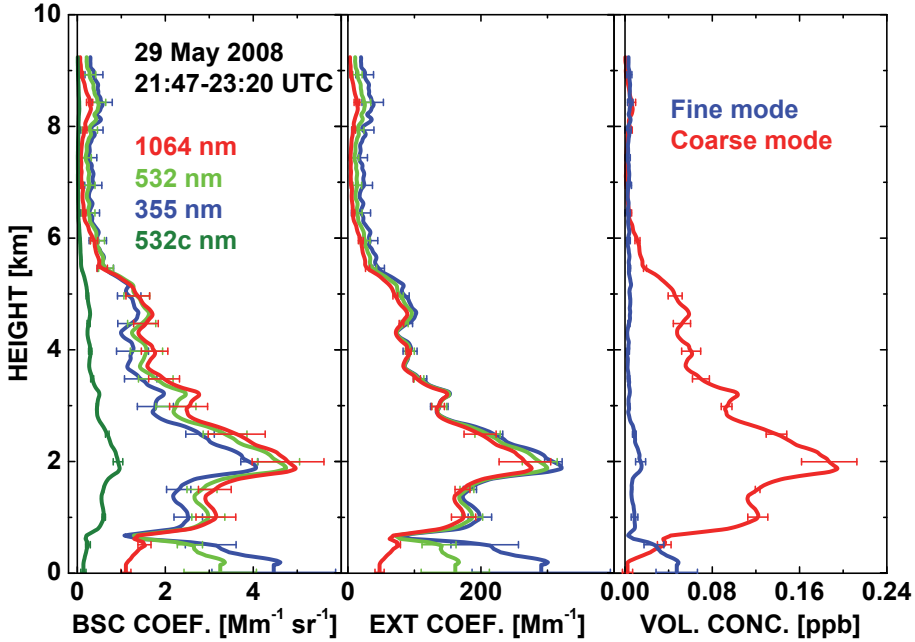

Fig. 3. Mean particle optical parameters (left: backscatter coefficient, center: extinction coefficient) for three laser wavelengths, backscatter coefficient for the cross-polarized 532-nm lidar channel (left, 532c nm, dark green), and particle volume concentration profiles (right) for fine-mode and coarse-mode fractions retrieved with the LIRIC method based on the lidar observations on 29 May 2008 shown in Fig. 2. The reference height is set to z_N = 9 km and the minimum measurement height is z_{N_0} = 150 m. The errors bars show the uncertainties (standard deviation) of the LIRIC results (see discussion in Sect. 3.1).

AMTD
6, 911–948, 2013

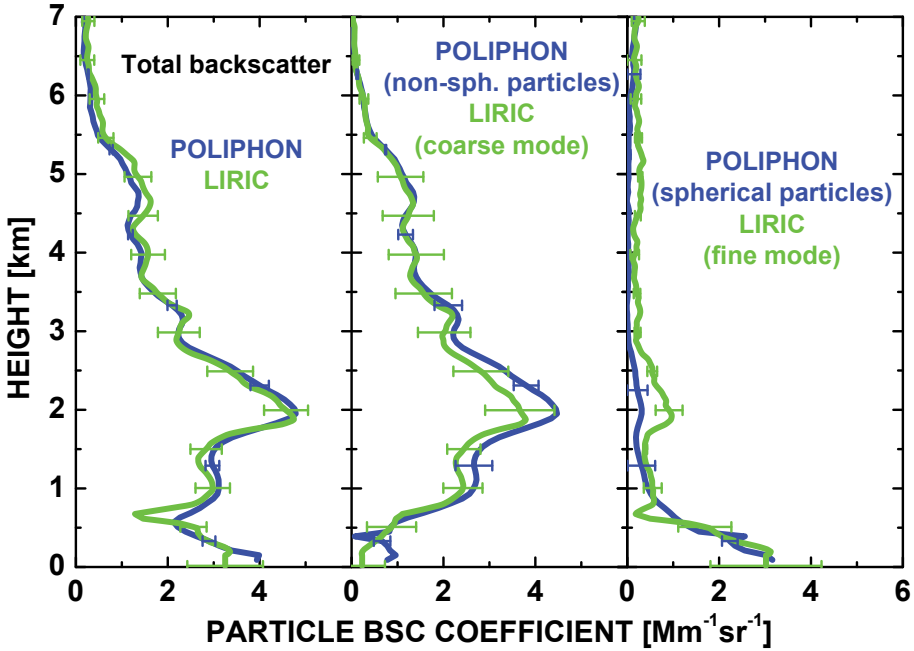

Fig. 4. Comparison of LIRIC- and POLIPHON-derived particle backscatter coefficients observed on 29 May 2008. The blue POLIPHON curves are taken of Fig. 2 of Ansmann et al. (2012). The error bars indicate the uncertainties of the retrieval products as discussed in Sect. 3.1 (LIRIC) and in Ansmann et al. (2011, 2012) (POLIPHON).

AMTD
6, 911–948, 2013

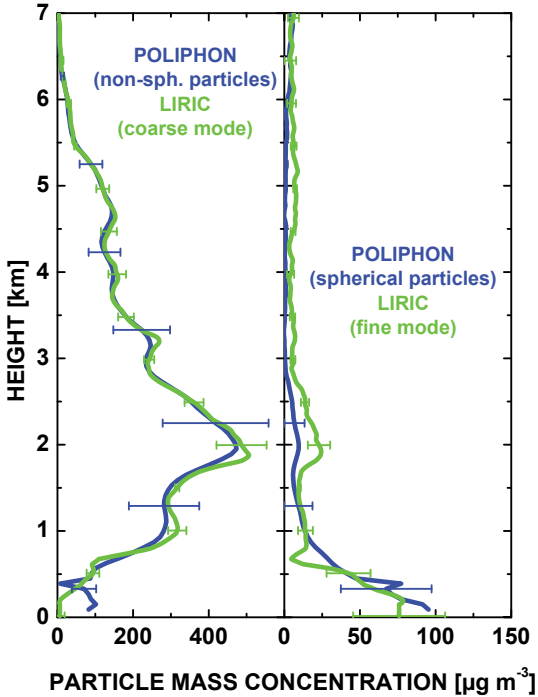

Fig. 5. Comparison of LIRIC- and POLIPHON-derived particle mass concentrations, observed on 29 May 2008. The blue POLIPHON curves are taken from Fig. 2 of Ansmann et al. (2012). Error bars indicate the uncertainties (one standard deviation).

AMTD
6, 911–948, 2013

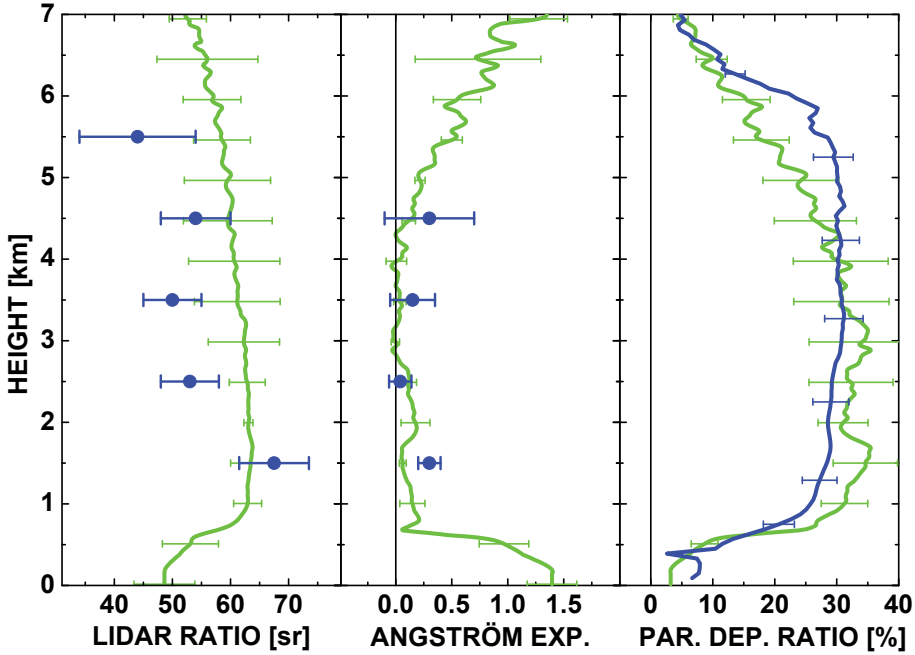

Fig. 6. Particle lidar ratio at 532 nm (blue circles), extinction-related Ångström exponent (355–532 nm) (blue circles), and particle depolarization ratio at 532 nm (blue curve) observed on 29 May 2008 with Raman lidar and derived by using the LIRIC profiles in Fig. 3 (green curves). Raman lidar signals are smoothed with window lengths of about 1000 m in the case of lidar ratio and Ångström exponent (blue symbols), so that mean values for 1000-m height intervals are shown. Errors bars indicate the uncertainties (one standard deviation). The depolarization ratio profile is given with 60 m resolution.

AMTD
6, 911–948, 2013

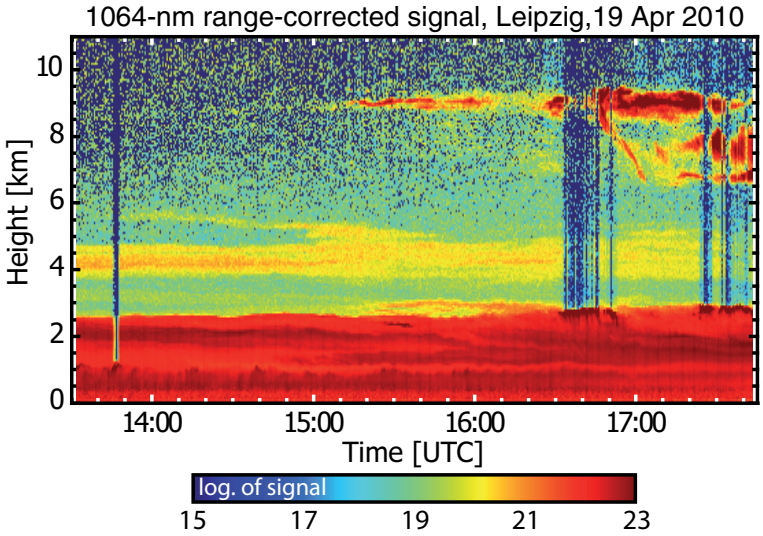

Fig. 7. Range-corrected signal at 1064 nm on 19 April 2010, 13:32–17:43 UTC. The vertical resolution is 60 m, the temporal resolution is 30 s. The 500-nm AOT was 0.7 up to 6 km height in the afternoon of 19 April.

AMTD
6, 911–948, 2013

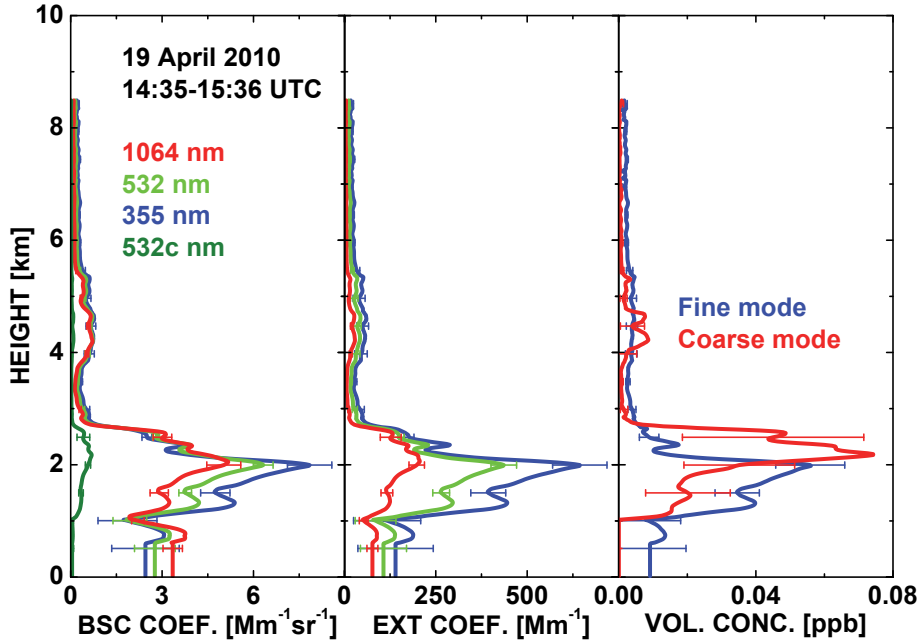

Fig. 8. Same as Fig. 3, except for a volcanic dust observation on 19 April 2010, 14:35–15:36 UTC with retrieval reference height of z_N = 8.25 km and minimum measurement height of z_{N_0} = 600 m.

AMTD
6, 911–948, 2013

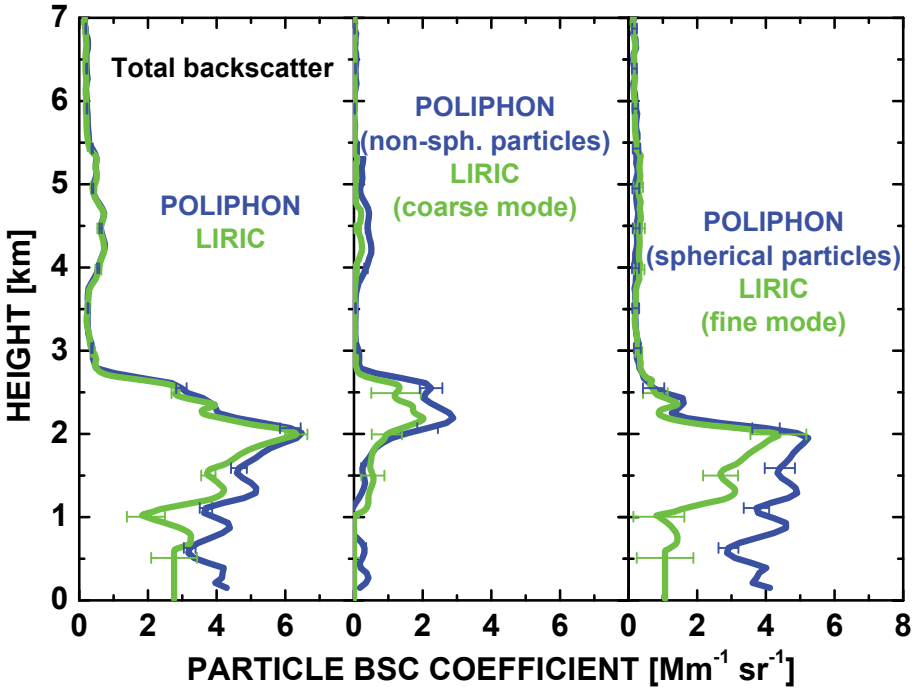

Fig. 9. Same as Fig. 4, except for a volcanic dust observation on 19 April 2010. The POLIPHON curves are taken from Fig. 4 of Ansmann et al. (2012).

AMTD
6, 911–948, 2013

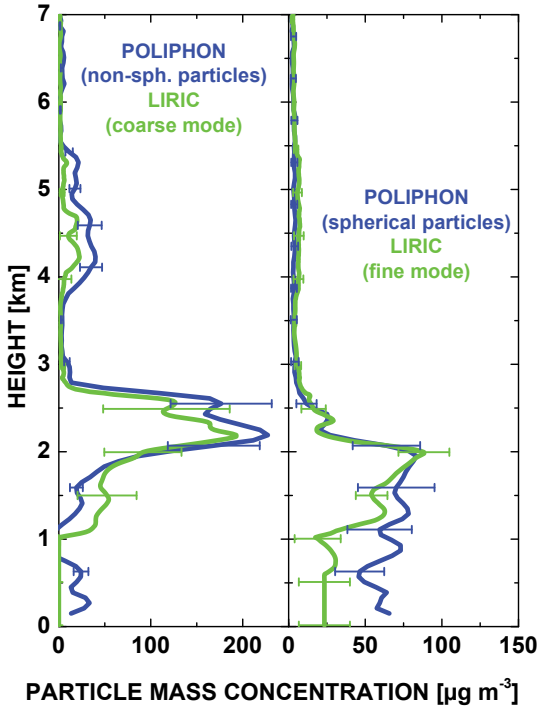

Fig. 10. Same as Fig. 5, except for a volcanic dust observation on 19 April 2010. The POLIPHON curves are taken from Fig. 4 of Ansmann et al. (2012).

AMTD
6, 911–948, 2013

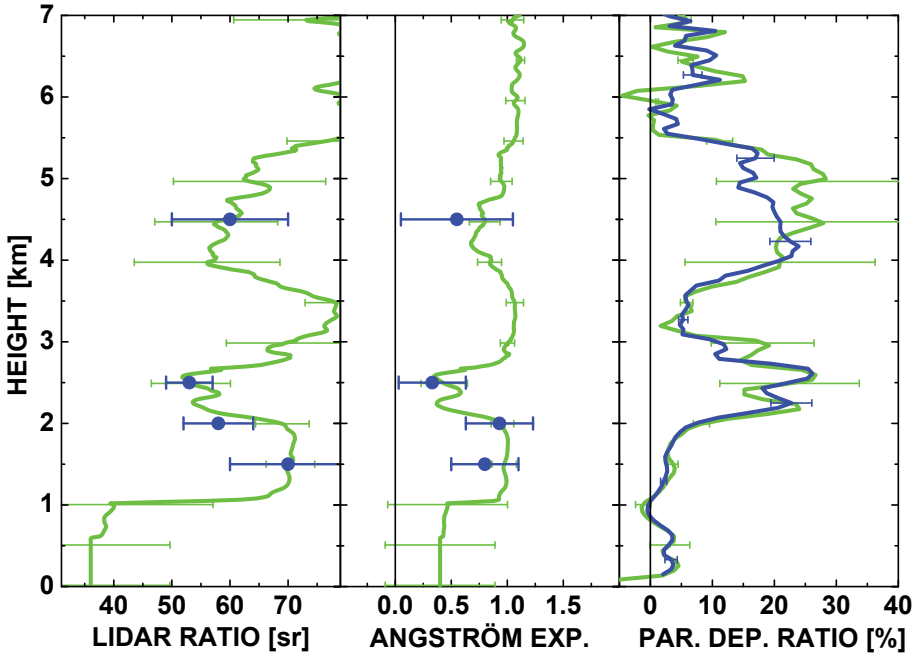

Fig. 11. Same as Fig. 6, except for a volcanic dust observation on 19 April 2010. Lidar signals are smoothed with 660 m vertical window length in the case of the Raman lidar solutions for the lidar ratio and Ångström exponent and averaged over two hours (13:30–15:30 UTC).

AMTD
6, 911–948, 2013